Online-Journals.org

iJOE International Journal of Online and Biomedical Engineering

iJOE | eISSN: 2626-8493 | Vol. 20 No. 12 (2024) | OPEN ACCESS

https://doi.org/10.3991/ijoe.v20i12.47773

PAPER

Analysis and Measurement of Tuberculin Skin Test Induration Using Deep Neural Network

Olubunmi Adewale Akinola[1], Joseph Folorunsho Orimolade[1], Akindele Segun Afolabi[2](✉), Habeeb Kehinde Shopeju[1], Emmanuel Adetiba[3–5], Adeyinka Ajao Adewale[3]

[1]Department of Electrical and Electronic Engineering, Federal University of Agriculture, Abeokuta, Nigeria

[2]Department of Electrical and Electronics Engineering, Faculty of Engineering and Technology, University of Ilorin, Ilorin, Nigeria

[3]Department of Electrical and Information Engineering, Covenant University, Ota, Nigeria

[4]Covenant Applied Informatics and Communication Africa Center of Excellence, Covenant University, Ota, Nigeria

[5]HRA of System Science, Durban University of Technology, Durban, South Africa

afolabisegun@unilorin.edu.ng

ABSTRACT

The World Health Organization (WHO) posited that tuberculosis (TB) is among the world's ten greatest causes of mortality. Early case identification and timely treatment could minimize TB morbidity and death rates. This study adopts the UNets model for automatically detecting TB in subjects by using a deep neural network to assess the size of induration after tuberculin was injected into their hands. In order to do this, two neural network models were fine-tuned utilizing pre-learned weights from the 2012 ILSVRC ImageNet. Algorithms were developed to perform semantic segmentation of induration and compare it to that of a reference object of a known dimension. This was used to classify the status of the subject as either positive or negative. A series of experiments performed demonstrated that the optimal selection of neural network hyperparameters may provide a satisfactorily high F1 score of up to 0.977.

KEYWORDS

tuberculosis (TB), induration, neural network, deep learning, tuberculin skin test

1 INTRODUCTION

The worldwide prevalence of tuberculosis (TB) illness has been very high. According to population surveys, 14 million people have a prevalent illness, resulting in around 10 million incident cases each year, of which approximately six million are identified and treated [1]. TB disease constitutes a major problem in most Sub-Saharan African (SSA) nations. This is due to poor case detection caused by delayed or missing diagnoses, resistance to medication, and problems associated with having the opportunity to receive of high-quality treatment. This in turn increases the risk of mortality, suffering, and devastating financial repercussions. Although it is agreed that early TB diagnosis and treatment are critical to its control, early identification of cases and prompt treatment also minimize TB morbidity and death [2]. Since TB can stay latent without discovery, it is extremely difficult to diagnose in its early stages. The fact that this sickness is not hereditary adds to its strangeness since there is no way

Akinola, O.A., Orimolade, J.F., Afolabi, A.S., Shopeju, H.K., Adetiba, E., Adewale, A.A. (2024). Analysis and Measurement of Tuberculin Skin Test Induration Using Deep Neural Network. *International Journal of Online and Biomedical Engineering (iJOE)*, 20(12), pp. 137–159. https://doi.org/10.3991/ijoe.v20i12.47773

Article submitted 2024-01-05. Revision uploaded 2024-04-03. Final acceptance 2024-04-05.

© 2024 by the authors of this article. Published under CC-BY.

of genetically tracking the condition [3]. This chest infectious disease (see Figure 1) is caused by the bacillus mycobacterium TB, which, according to the World Health Organization (WHO) estimations, is among the world's ten greatest causes of mortality and the main source of death caused by one contagious agent. It has ranked top on the list of the most lethal infectious illnesses for the last seven years [4].

Fig. 1. Tuberculosis is a disease of the chest region

There are two classifications of TB [5]: latent and active. Latent tuberculosis infection (LTBI) is an asymptomatic, non-contagious clinical condition, while active TB illness is defined by the presence of clinical symptoms resulting from an infection that may occur in various organs, is a symptomatic clinical condition. While the organism that causes TB, mycobacterium TB, may affect many different body areas, pulmonary TB is generally the transmissible variant.

Although CT imaging is becoming more popular, the basic chest X-ray is still a popular imaging modality in TB screening regimens, especially in low- and moderate-resource areas. The difficulty with TB is that it appears in a range of sizes and forms with varying image intensities. This can be masked or confused by superimposed or enclosing lung structures. There are distinct TB patterns (for example, nodule clusters and cavities) as well as anatomical distributions that suggest a TB etiology (e.g., parahilar, costophrenic angles, apical predominance) [6].

A combination of associated symptoms and a thorough review of the medical history of the patient are used to make the diagnosis of TB illness. Early TB diagnosis is complicated by the delayed bacterial reproduction that takes place in the patient's lungs before the illness manifests itself in symptoms. Several tests are currently available for the diagnosis of TB, including liquid culture with drug susceptibility testing (DST), chest X-ray, conventional light microscopy, light-emitting diode (LED) fluorescence smear microscopy, lipoarabinomannan (LAM) lateral flow assay, and first-line (FL) line probe assay. Sputum cultures, Xpert MTB/RIF, and microscopic inspection are used to diagnose pulmonary TB early. A DST is used, however, to diagnose drug-resistant strains. The conventional techniques for determining illness and medication resistance are laborious, time-consuming, and need extra time for report interpretation [7].

Digital image processing was used by Pedro and Barfeh [8] to study a tuberculin skin test checker. They used the strategy of making four markings with a pen on the induration's margins in what would be called the north, south, east, and west. Moreover, a scale was available to be put on the arm before taking images. The images are then subjected to a variety of image processing procedures, such as cropping, grayscale conversion, and the use of Gaussian blur to reduce image noise. The four edges and the scale are then identified using the canny edge detection technique.

They use morphological dilation and erosion to increase the visibility of the edges, which may be faint. They then perform image localization using contour finding to locate the scale's position and its edges. The goal was to determine the image's pixel size and then calculate the conversion factor between it and the scale's actual size. The Euclidean distance between the edges was then calculated once they had located the edge markers. The conversion ratio found from the scale was then used to convert the pixel into the actual distance because this distance is in pixels. They then conclude on the positivity or negativity of TB using the actual distance acting as the diameter of the induration.

Artificial intelligence (AI) and machine learning (ML) are increasingly being applied in various sectors, including the educational sector [9]–[14], the telecommunications sector [15]–[19], and the medical sector [20, 21], just to mention a few. It has been used in the healthcare industry to address issues with diagnostic support systems, medical image analysis, and public health. To detect teeth images with and without cavities, the researchers in [22] employed four pre-trained deep CNNs: VGG-16, VGG-19, DenseNet-121, and Inception V3. The proposed technique achieved 98.3% accuracy by combining preprocessing methods such as histogram equalization and Sobel edge detection with the VGG-16 model, stochastic gradient descent (SGD), and Nesterov's momentum algorithm.

Since 1999, when El-Solh et al. published their results, other strategies for treating TB have been put forward. For them, the primary source of information was medical imaging. Improvements in this area have made it possible to more accurately diagnose thoracic disorders such as TB, pneumonia, asthma, and cancer. By using the useful data that is now accessible, like data from molecular biology or clinical information, researchers have often employed specialized ML models in health systems to improve TB diagnosis. Through various architectures like self-organizing maps, multilayer perceptrons (MLP), and adaptive resonance theory (ART), coupled with fuzzy models in the fuzzy-ART approach, it aids clustering and detection in risk groups for pleural TB and pulmonary TB. Artificial neural networks (ANNs) have been particularly helpful in integrating ML into the diagnosis of TB. Researchers have collected respiratory acoustic signals and other clinical information to aid medical practitioners in their regular work [23]. This study entails the application of UNets to the problem of measuring tuberculin skin induration by fine-tuning a UNet model on the sourced dataset and applying the model for image segmentation, after which the pixels were extracted and the induration size was calculated.

2 RELATED WORKS

Several studies have applied smartphones to the detection of TB [24, 25, 26]. Dendere et al. [27] used a mobile smartphone to photograph artificial skin indurations on 10 participants that ranged in size from 4.0 to 19 mm. Next, they used photogrammetry software to rebuild the indurations in three dimensions. The size of each induration was assessed by an expert TST reader using the accepted clinical technique. Both the skilled reader and a novice observer used the program to gauge the magnitude of each induration. Using the intra-class correlation coefficient, the agreement between measures produced by conventional clinical and image-based approaches was evaluated (ICC). The image-based method's inter- and intra-observer agreement were similarly assessed. With an ICC value of .965, the results demonstrated high agreement between the standard and reader-performed image-based measures. Excellent inter- and intra-observer agreements show that their suggested strategy does not need prior knowledge of reading TSTs.

There is a growing interest in applying AI-based software techniques to identify pulmonary tuberculosis (PTB) with the aim of increasing diagnostic accuracy while at the same time, lowering costs. Several studies [28]–[37] have used AI to tackle the difficult task of predicting and assessing TB in TB diagnosis. The concept of pattern recognition was introduced with the development of neural networks (perceptrons and their upgraded variants), which could identify structural patterns in chest X-ray pictures and aid in diagnosis.

Hrizi et al. [38] applied the support vector machine (SVM) ML algorithm to solve the TB diagnosis problem. They used two novel methods in accordance with the GA to enhance the SVM classifier's performance. In order to ensure the maximum accuracy level for the entire training and testing phases, an adaptive GA was used as the first approach for the choice of the perfect parameters among various values. The second strategy was employed to pick a minimal number of the original features with a view to preventing overfitting as well as reducing the data's dimensionality. The results of their experiments demonstrate that their modified SVM classifier was superior to many other existing classifiers used in classifying tuberculosis.

The authors in [39] applied decision trees to TB diagnosis. They developed a unique technique that employs segmentation, feature extraction, and classification in three stages to identify TB in chest X-ray (CXR) pictures. They used the Weiner filter in a CXR to separate out and reduce impulsive noise. The features were taken from CXR pictures and trained using the stacked loopy decision tree (SLDT) classifier, which is a type of decision tree classifier. A three-phased technique was used for the classification procedure, and the ROI-based morphological approach was used. Chromatic and Prewitt-edge highlights were used to retrieve feature information. Experimental findings showed that TB could be correctly predicted in CXR utilizing the SLDT. In [40], the authors applied the random forest classifier to successfully detect TB. Compared to the Naive Bayes classifier, the performance of their approach, which was a modified random forest method produced high accuracy.

By the start of 1990, pattern recognition algorithms were responsible for artificial neural networks (ANN) beginning to help in the diagnosis of TB [7]. In order to distinguish between the various interstitial lung illnesses, as well as TB, a neural network was developed in 1990. Ten instances for each of the nine kinds of lung illnesses were used to create the training dataset. The model performed well and produced excellent results, indicating that ANN has great promise for lung illness computer-aided diagnosis. The first automatic neural approach was developed in 1998 to recognize the TB bacillus in auramine-stained sputum smears.

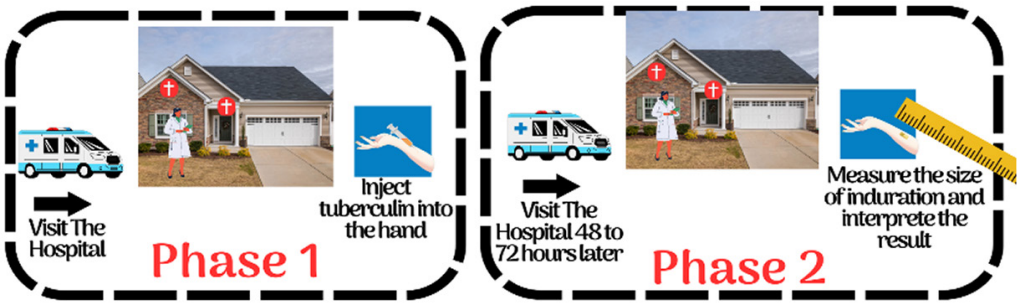

Fig. 2. Traditional tuberculosis diagnosis procedure

The model's sensitivity was 93.5%, with the goal of quickly and reliably diagnosing TB while lowering health hazards for personnel handling smear slides.

Today, several studies on TB diagnosis based on convolutional neural networks could be found in the literature [41]–[44].

3 METHOD

In this work, a method that does not require the patient to visit the hospital twice was proposed. The traditional manual TB diagnosis method is illustrated in Figure 2, while our proposed automated diagnosis method is illustrated in Figure 3. It can be observed in Figure 3 that in the first phase, the patient visits the doctor to get tuberculin injected into their hand. In the second phase, the patient snaps the picture of the induration together with a reference object (in this case, a credit card), uploads it to an online platform, and gets the interpretation after some seconds.

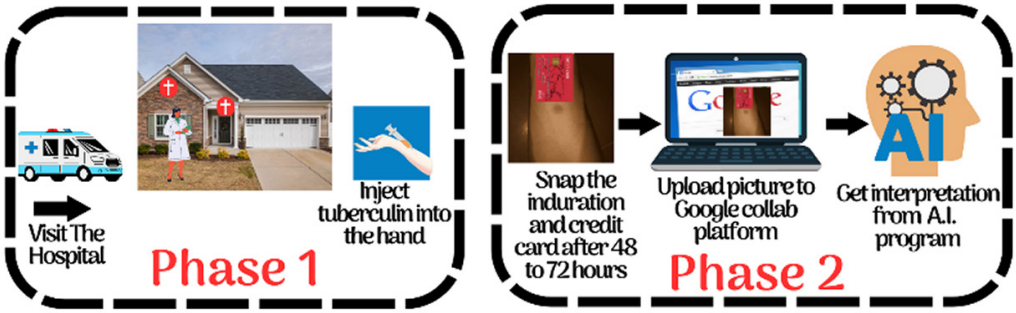

Fig. 3. Proposed solution

In order to implement the phase 2 portion of Figure 3, it is necessary to build and train an artificial intelligence model, and the model must be user-friendly enough to be operated by non-technical users who cannot navigate a programming language platform. The user interface should allow an image to be uploaded, then extract the region of the credit card and the region of the industry. Next, the application should display the estimated measurement and its interpretation to the user.

The functional units of our proposed phase 2 are therefore divided into two parts, namely:

i) The frontend
ii) The backend

3.1 The frontend

The frontend section is the interface through which the user interacts with the system. This interface, in this study, has been developed using: (i) Streamlit; (ii) the VGG Image Annotator (VIA); and (iii) the ImgAug library. Streamlit is a platform that makes it easy to build data-intensive web applications and share them with people without frontend development experience [45]. VIA is a free image annotation project that allows annotating images, audio, and videos from the web browser. The ImgAug library is the main library used for performing image augmentation in this project, since it has the functionality to modify images in multiple ways. The Albumentations library is also used for augmentation when loading an image into a model.

3.2 The backend

This is the server part of the system where the processing of the uploaded image is performed and the interpretation of the result is provided. In this paper, the backend program resides in the cloud and is powered by the Google Collaboratory platform.

Backend libraries. Unlike the frontend, which integrated multiple application packages, the backend was programmed in Python and uploaded to the Google Collaboratory platform. It is important to mention certain libraries that performed major tasks in the backend. These libraries are: (i) segmentation models; (ii) Keras; and (iii) OpenCV. The Python library segmentation models implement various image segmentation networks, such as the U-Net, FPN, Linknet, PSPNet, and EfficientNet [46]. Backbones with weights learned from the 2012 ImageNet dataset are also included in the segmentation models. The EfficientNet [47], which was regarded as more accurate and efficient than other ConvNets at the time of this study, served as this study's backbone. Keras is a deep learning library that simplifies the creation of neural networks [48]. Computer vision capability is provided via the open-source computer vision library (i.e., OpenCV) [49].

Data sourcing and engineering. Neural networks are primarily driven by data, and it is often said that the richer the data, the better the model [50]. So, gathering the data, cleaning it if required, and transforming it into the proper form before feeding it to the model are crucial. Getting image data for biomedical processing is a big challenge, and many biomedical data science projects have to proceed with little data. This issue served as the impetus for the development of the U-Net model, which works well with sparse data, as seen in biological use cases [51]. Thirty-three (33) photos were obtained from Google, Reddit, Twitter, and Facebook to serve as the induration data. To get an extra 23 photographs, a graphics artist assisted in superimposing some of the indurations from the originally sourced images on new images of an ordinary arm. The deposit photos platform was the major source for locating reference object data (credit cards), which comprises 103 pictures.

Data augmentation. Massive amounts of data are required for neural networks to thrive and generalize effectively enough to tackle real-world issues. Yet, since data is always a barrier, data augmentation has proven to be a helpful method of creating extra data while avoiding the danger of overfitting the model [50]. Data augmentation is a method of increasing the amount of a dataset by changing each data point (in this example, an image) to avoid overfitting and create more variation in the data. Rotation, cropping, affine transformations, contrast, and pixel dropout are some picture augmentation procedures that may be utilized. Overlaying skin swelling on arms is also an excellent way to supplement and create fresh images for training; graphics specialists assisted in making this overlay as realistic as feasible.

A collection of 56 photos was utilized to train a machine that conducts semantic segmentation on skin indurations. Figure 4 depicts a sample of the industrial photo dataset gathered from the internet. This dataset was divided into 12 photos for testing, 12 for validation, and 32 for training; the training dataset was up sampled into 5632 images using data augmentation.

Credit cards were selected as the paper's reference object since they have a worldwide standard size of 3.370 in × 2.125 in [52]. These photographs (see Figure 5) were obtained from stock photography websites. A dataset of 103 photos was used to train a machine that performs semantic segmentation on cards. Figure 5 shows a glimpse of the internet-sourced credit card picture dataset. This dataset was divided into 16 photos for testing, 16 for validation, and 71 for training; the training dataset was up sampled into 3,621 images using data augmentation.

Fig. 4. Preview of the skin induration image dataset

Fig. 5. Preview of the credit card image dataset

Data annotation. Data annotation is required in this study to get the points around the swelling and construct the correct segmentation for a particular picture. The annotation procedure produces a vector of the points picked by the annotation tool, which may be fed into the data loader or used to produce a segmented version of the picture to train the model. Figure 6 depicts an example of an ongoing data annotation job in an industry. After processing the annotation points, Figure 7 displays a segmentation picture of the induration in Figure 6.

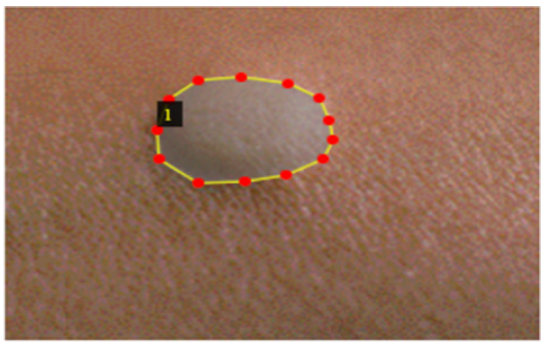

Fig. 6. Screenshot of image annotation ongoing with VIA tool

Fig. 7. Grayscale image resulting from image annotation

3.3 Model training

Computer vision operations such as object detection and object localization are important for semantic segmentation, but in this study, it is important to localize down to the pixel level to train a model before the segmentation mask can be predicted. The segmentation models library provides pre-trained weights from the 2012 ILSVRC ImageNet dataset [46], which can be used to modify the weights gradually to fit the desired data. This is known as transfer learning, and it is useful for this project due to the lack of sufficient data. Training is done on the dataset, modifying the weights well enough to provide the desired segmentation.

A neural network's hyperparameters are characteristics that affect how the network trains the model on the data. To acquire the greatest outcomes from the model, it may be adjusted and tested. Every project has a different set of ideal values for various hyperparameters. While there are several hyperparameters, the ones used in this study are the *activation function*, *batch size*, *learning rate*, and *loss function* [46].

Activation functions cause a certain state to occur when a particular value is passed to them. Based on the input, a perceptron's state may be set to either 1 or 0. There are several activation functions, each with a specific use case, including *softmax*, *tanh*, *sigmoid*, and *rectified linear unit (ReLU)* [53]. The trained models in this study perform binary segmentation; hence, the sigmoid activation function is used as the activation function for the output layer. Such activation functions may still be utilized in the hidden layers of the U-Net, despite the fact that they are not modifiable in the segmentation model's library. Sigmoid is a function that limits its range to between 0 and 1, allowing it to be used to solve binary classification issues by predicting whether a picture includes an item or not. It can be used in the last layer of a neural network to predict whether an induration is present in a picture.

Neural networks need many images to have the right weights and generalize enough for making predictions, but the computer can quickly run out of RAM. Batch size helps to deal with this problem as the images can be passed through the neural network in batches instead of all at once. A general starting point for the batch size is 32, but experiments can be done with batch sizes 8, 16, 64, and 128. Due to the nature of the pre-trained model used in this study, batch sizes 8 and 16 were used to avoid out-of-memory (OOM) errors.

Every time an epoch is finished, the learning rate is measured by the magnitude of the steps made during gradient descent as the weights get closer to the global minimum. Optimization methods like Momentum, Root Mean Square Prop (RMSProp), or Adaptive Moment Estimation may be used to enhance or reduce it. For experimentation, learning rates of 0.1, 0.01, 0.001, and 0.0001 are more typical numbers. Experiments were used to choose the learning rate used in this study, as will be discussed in a later section.

Based on a convex solution, the gradient descent process continuously modifies weights until they approach a global minimum. For gradient descent optimization, a number of techniques are available, including mini-batch gradient descent, batch gradient descent, and stochastic gradient descent. The Adam algorithm was used in this study since it produces the best results. The goal of machine learning is to get a model's predicted value as close to the real value as possible. The technique used to determine this is the loss function, and the lower the value produced by the loss function, the better. There are many loss functions, but dice loss and focal loss are often used for semantic segmentation.

3.4 Implementation of the backend

The core of the backend implements a neural network algorithm for segmenting the uploaded image, extracting the pixel size of the induration portion of the image, and using this to achieve a multi-class classification. The algorithm is presented in the flowcharts shown in Figures 8a and b. Figure 8a is the main program, while Figure 8b is a subroutine that receives an image as an argument, segments the image, and returns the image pixel size to the main program.

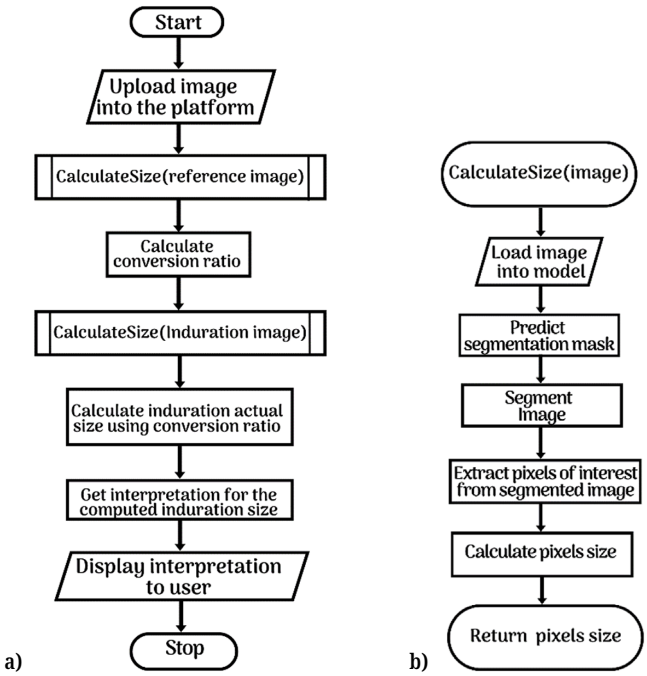

Fig. 8. (a) The flowchart of the main program; (b) The flowchart of the subroutine for performing image segmentation

The main program and subroutine. The main task performed by the subroutine is image segmentation. The neural network architecture employed for realizing it in this paper is the U-Net. It is referred to as U-Net because of its U shape, which can be seen in Figure 9. This architecture has different layers needed to down sample the image to get the notable features and then up sample to regain the initial spatial dimensions while performing the segmentation.

This architecture involves four significant operations: convolution, copy and crop, max pool, and up convolution [51]. The convolution operation allows the network to produce feature maps from the input images (i.e., the induration and the reference images) matrix in order to discover patterns in the images. The copy and crop operation aids in the duplication of feature maps on the left side of the U before they are concatenated with feature maps on the right. Cropping of the left feature maps to suit the spatial dimension of the right feature maps is also required by the architecture.

The max pool function aids in dramatically reducing the spatial dimensions of feature maps by selecting the most important pixels in the feature map. The up-convolution operation restores the feature maps' spatial dimensions. Bilinear interpolation or transpose convolution may be used to do up convolution. Up convolution differs from deconvolution (which reverses convolution); this allows

segmentation to provide an output that is not identical to the input image but has the same spatial dimensions.

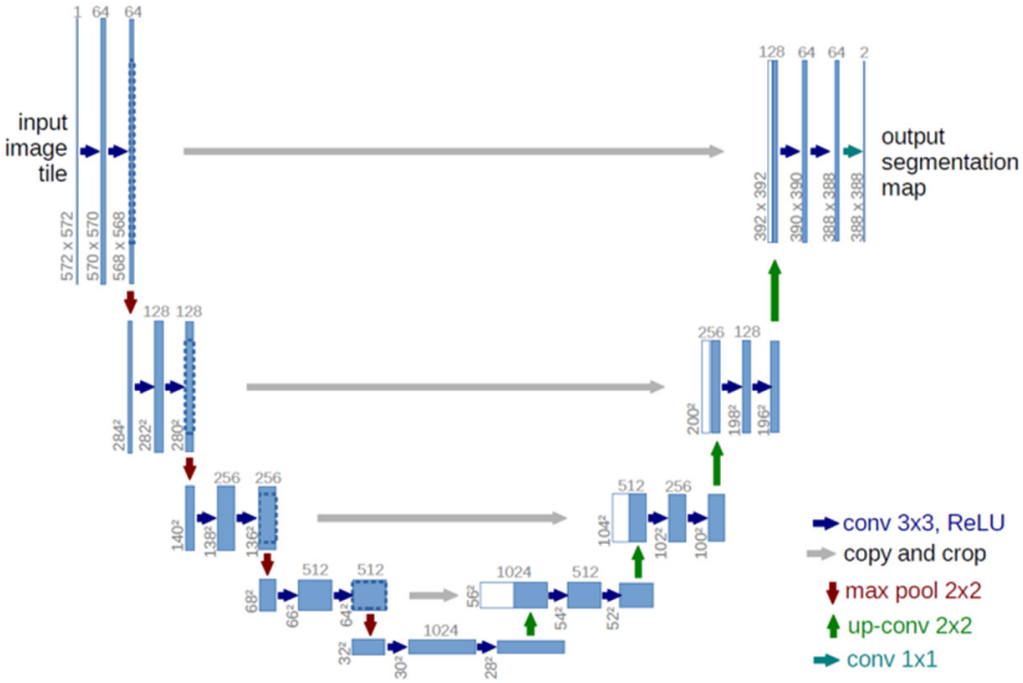

Fig. 9. Architecture of the U-*Net*

The main program. The main program performs 2 tasks, which are:

i) Computing the induration size; and
ii) Classification based on the interpretation of induration size.

Computing the induration size. The user interface, which was built using Streamlit, loads up and waits for an image from the user. On getting user input, the main program calls the subroutine twice to create two models. During the first call, the reference model is created, which segments the reference object image, which in our case is a credit card. During the second call, the induration model is created, which segments the induration image. When the reference object is segmented, its pixel size is extracted for purposes of calculating the pixel-to-real size conversion ratio. Later, when the induration is segmented, it is converted into a real size using the conversion ratio calculated earlier. The pixel size of the reference object in the image is compared to its actual size, known globally. This ratio is then used to extract the actual induration size [54]. The actual size of the induration can then be obtained by multiplying the pixel size of the induration by this ratio. The measurement accuracy is expected to be reduced because of this conversion; however, the results should come close to the actual size of the segmentation. The real size of the induration is computed as:

$$RI = PI \times \frac{RR}{PR} \tag{1}$$

where:
RI is the real size of the skin induration
PI is the pixel size of the skin induration

RR is the real size of the reference object
PR is the pixel size of the reference object

Classification based on the interpretation of the induration size. When the measurement of the induration is complete, the next step is to analyze and interpret. The interpretation is based on the following categories of induration size:

a) Category I
This category includes people with an induration size that is less than 5 mm. Such a person has little or no reaction to the tuberculin; hence, they are deemed to be negative for latent tuberculosis.

b) Category II
This category includes people with an induration size that is greater than or equal to 5 mm but less than 10 mm. A person with an induration size in this category is deemed to be positive for latent TB if they: have human immunodeficiency virus (HIV); recently came into contact with active TB patients; are organ transplant recipients; and are at the end stage of renal disease.

c) Category III
This category includes people with an induration size that is greater than or equal to 10 mm but less than 15 mm. A person with an induration size in this category is deemed to be positive for latent TB if they; are a recent arrival (under five years) from high-prevalence countries; are employees or residents of high-risk congregate settings (e.g. hospitals, homes, nursing, homeless shelters and prisons); have high-risk clinical conditions (e.g., leukemia, prolonged corticosteroid therapy, end-stage renal disease, diabetes, low body weight, and chronic malabsorption syndromes); and are children below four years or children including adolescents open to adults in high-risk categories.

d) Category IV
This category includes people with an induration size that is greater than 15 mm. A person with an induration size in this category is deemed to be positive for latent TB if they have no known risk factor for tuberculosis.

For experimental purposes, U-Net neural network models are trained using EfficientNet B1 and B4. The EfficientNet ranges from B0 to B7, with B0 being the smallest model with the lowest accuracy and B7 representing the biggest model with the best accuracy. B1 was selected to test the outcomes of a lightweight model that does not demand a lot of memory resources from a server, while B4 was chosen to test how much accuracy can be obtained despite utilizing a lot more memory. The Adam optimizer was selected as the model's optimization mechanism, and learning rates ranging from 0.01 to 0.00001 were tested. The studies employed a batch size of 8, with 16 also being explored for EfficientNet-B1. When EfficientNet-B4 was run with a batch size of 16, out of memory (OOM) issues occurred. Credit card models were trained using a variety of hyperparameters, and the most promising hyperparameters were batch-size, learning rate, and number of epochs, and they were varied for various EfficientNet backbones utilized to train the induration models.

4 RESULTS AND DISCUSSION

This section presents the results obtained in this work as well as the discussion of the results.

4.1 Model evaluation

After training, the models were assessed using the test dataset obtained at the start of the study. During the assessment, the segmentation model's library gives three metrics: loss, intersection over union, and F1 score. Tables 1 and 2 show the evaluation results for the credit card model and the induration model, respectively. The training results reveal that the EfficientNet-B4 models have a higher intersection over union and F1 models. Another discovery is that when a lower learning rate, such as 0.0001, is utilized, it takes longer for the models to converge. Nevertheless, the results of a considerably higher learning rate, such as 0.01, are not as striking and might be interpreted as the model having difficulties arriving at an optimum point. The best results are obtained for learning rates as high as 0.001 and as low as 0.0001.

Table 1. Evaluation of the *credit* card model on the test dataset

EfficientNet	Batch Size	Epochs	Learning Rate	Loss	Intersection Over Union Score	F1 Score
B1	8	20	0.01	0.2909	0.6798	0.7768
B1	8	20	0.001	0.185	0.7794	0.8198
B1	8	20	0.0001	0.0897	0.8952	0.9363
B1	16	20	0.01	0.1114	0.8382	0.8766
B1	16	20	0.001	0.0965	0.6327	0.9294
B1	16	20	0.0001	0.1034	0.8045	0.8679
B4	8	20	0.01	0.7298	0.6327	0.7318
B4	8	20	0.00001	0.143	0.8815	0.9277
B4	8	20	0.0001	0.0716	0.9029	0.9448
B4	8	20	0.001	0.0961	0.8799	0.9255

Table 2. Evaluation of the skin induration model on the test dataset

EfficientNet	Batch Size	Epochs	Learning Rate	Loss	Intersection Over Union Score	F1 Score
B1	8	20	0.01	0.0457	0.9332	0.9651
B1	8	20	0.001	0.0377	0.9351	0.9662
B1	8	20	0.0001	0.3713	0.9449	0.9714
B4	8	20	0.001	0.0229	0.9555	0.977
B4	8	20	0.0001	0.0371	0.9352	0.9662

4.2 Model inference

Looking at the metrics from training the credit card and induration models in Tables 1 and 2, one can observe that learning rates of 0.001 and 0.0001 generated good results. As a consequence, models trained with these hyperparameters and EfficientNet-B4 are selected to visually verify model inferences. Figure 10 depicts the picture used for credit card inference, and Figure 11 shows the segmentation

results following model inference. It is important to mention that both the front face and the back face of the credit cards are used in training the model, as shown in Figure 10. This is because the intended end users (the patients) of the model are not trained professionals and, therefore, may not be careful enough to comply in a situation where there is a stringent restriction regarding the face of the credit card that must be used. Hence, training with both faces generalizes the resulting model so that it performs acceptably with both the front and back faces of the credit card during the deployment phase.

Fig. 10. Sample image with credit cards only

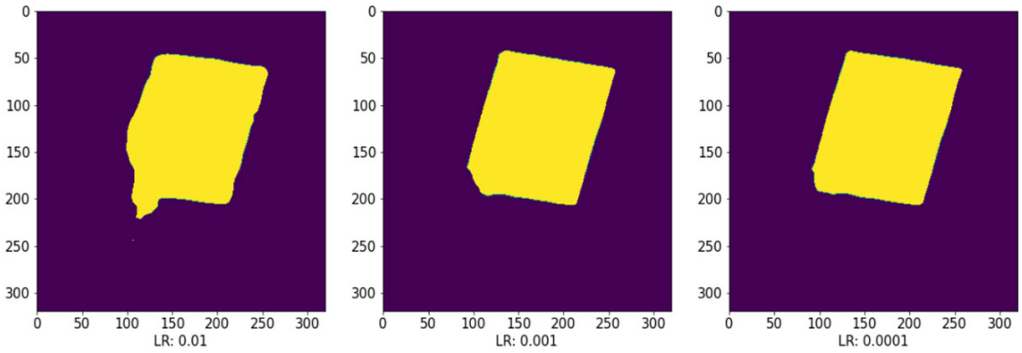

Fig. 11. Semantic segmentation for Figure 10

When evaluated on photos randomly picked from the validation dataset, the model trained with a learning rate of 0.0001 gives a more aesthetically pleasing outcome than the model trained with a learning rate of 0.001. Figure 12 depicts the picture utilized for induration inference, and Figure 13 shows the segmentation results following model inference.

Fig. 12. Sample image with induration only

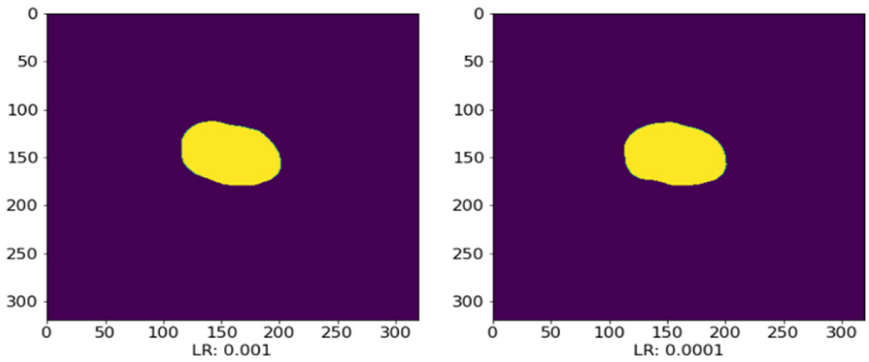

Fig. 13. Semantic segmentation for Figure 12

In Table 2, the metrics from the induration model show that learning rates of 0.001 and 0.0001 both achieved adequate outcomes. As observed with the credit card model, the model trained with a learning rate of 0.001 has a modest advantage over the model taught with a learning rate of 0.0001.

Fig. 14. Sample image with credit card and skin induration

When evaluated on photos randomly picked from the validation dataset, the model trained with a learning rate of 0.0001 generates more aesthetically pleasing results. Since both models were trained on independent datasets, one area of worry is their ability to perform effectively in photos, including a credit card and an induration. A simple overlay of the card over a picture with swelling was used to produce several example images, one of which is illustrated in Figure 14. Figure 15 shows the segmentation results from both models.

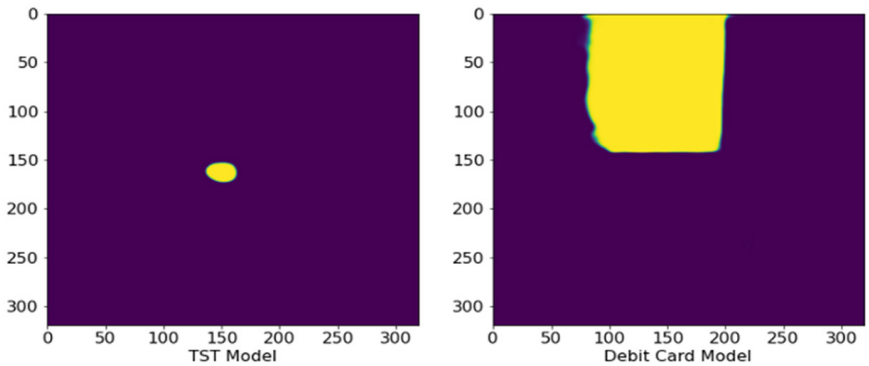

Fig. 15. Semantic segmentation for Figure 14

The findings in Figure 15 show that the models can conduct segmentation on pictures with a card and an induration. Unfortunately, the models, particularly the credit card model, may not be completely reliable in every case. Figure 16 shows an induration and a card overlay as examples, and Figure 17 shows segmentation results from both models.

Fig. 16. Sample image 2 with credit card and skin induration

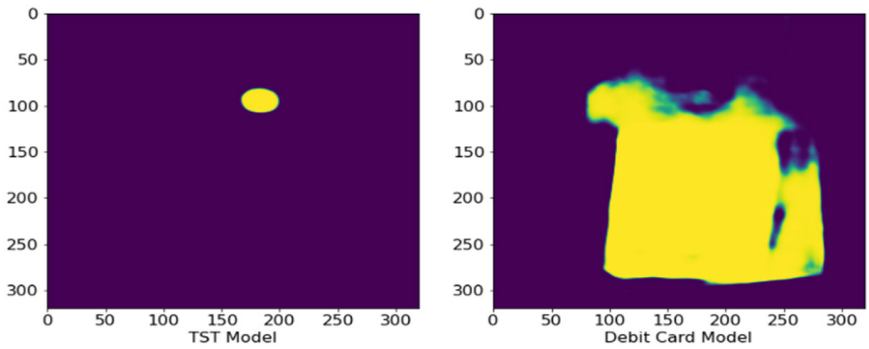

Fig. 17. Semantic segmentation for Figure 16

As can be seen, the swelling segmentation is precise, but the credit card segmentation is not. Improvements on both models are feasible by acquiring a big enough dataset that comprises both the induration and the credit card. Certain post-processing processes, such as erosion, may enhance the results. Since the credit card model detects regions, it should not, erosion reduces object size and noise. Figure 18 is the result of doing erosion on the segmentation from the credit card model.

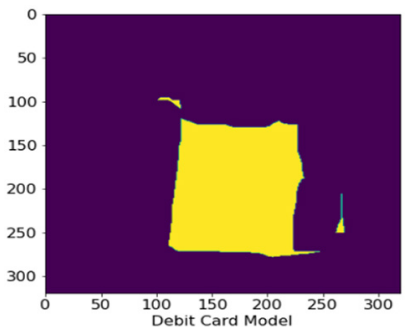

Fig. 18. Denoised semantic segmentation for Figure 17

The results suggest that erosion may lower the number of incorrect regions detected by the model. As a result, it may be utilized to address the problem of poor segmentation with considerable false positives. Unfortunately, its utilization cannot surpass the results of a model trained on a high-quality dataset.

After the creation of the model, an interface was designed to make the model usable for non-technical people who are unable to traverse the Google Colab notebook. This tool enables you to submit a picture and then extract the credit card and industry regions. The program then shows the user the estimated measurement and its explanation. Figures 19 and 20 depict the interface's workflow.

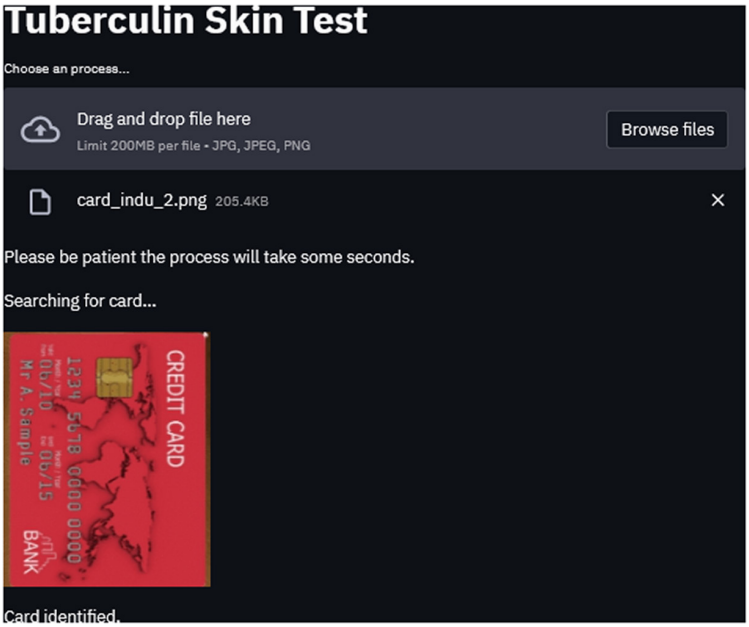

Fig. 19. Credit card identification interface on Streamlit

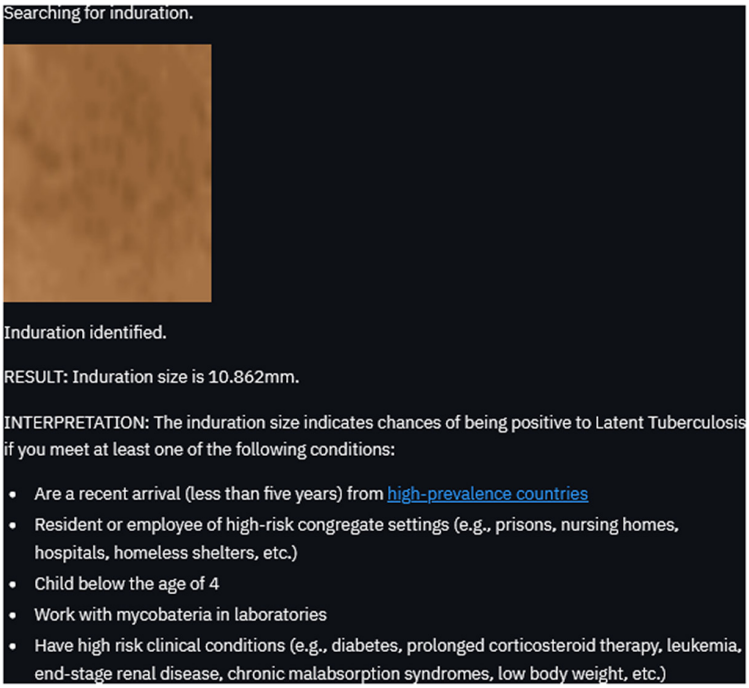

Fig. 20. Induration identification and analysis interface on Streamlit

4.3 Discussion

The automated diagnosis of TB by using a deep neural network to assess the size of induration after tuberculin has been injected into the hand looks promising; however, it is important to take cognizance of its implications for clinical practice as well as its limitations.

Implication for clinical practice

Effectiveness and speed. The U-Net employed in this study ensures that the speed and efficiency of screening for TB will be substantially improved. It will save healthcare practitioners a significant amount of time and provide faster diagnosis and treatment. This, in the long run, will help reduce the pressure on medical facilities in situations where the available medical resources are outnumbered by the population size of patients seeking medical service.

Accuracy. The F1 score of 0.977 achieved in this work implies that false positive and false negative predictions are low thanks to the deep neural network employed. A well-trained and tested U-Net achieves high accuracy in terms of prediction of induration size, thereby substantially reducing the mistakes that sometimes occur when measuring it manually.

Standardization. The proposed U-Net would allow for easy standardization of measuring processes across settings while also being highly reproducible by different healthcare providers, resulting in reduced variation in diagnosis and increased consistency of management for patients.

Limitations and future research direction

Small-size dataset. There was a limited amount of data available for developing the proposed model. In all, 56 induration images were used (32 images for training, 12 images for testing, and 12 images for validation). Due to the small size of the data, the training data had to be up sampled to 5,632 images. In our future work, a sufficiently large dataset will be sourced.

Poor generalizability of the trained model. The deep learning model was trained with data obtained from a certain population and under controlled imaging conditions, which makes it weak in terms of generalizability. Our future study would focus on generalizing the proposed work across datasets, not just in the area of various patient demographics but also of diverse imaging modalities in general.

5 CONCLUSION

This paper presents a novel approach for the automatic detection of TB in subjects by classifying the size of induration after tuberculin has been injected into their hand. In order to achieve this, two neural network models (induration and reference models) were constructed using pre-learned weights from the 2012 ILSVRC ImageNet. Both models' segmentation results serve in determining the magnitude of a Tuberculin skin test swelling. The swelling size is compared to the size of a reference object before arriving at an inference. The credit card has been selected as the reference object in this paper due to its universally standard dimension. The reference object's semantic segmentation result aids in calculating a number for translating pixel size to real size. This number aids in estimating the swelling size based on the semantic segmentation result obtained for the induration. Results of a series of experiments revealed that an F1 score of up to 0.977 is realizable through an optimum selection of neural network hyperparameters. This work suffers some limitations in terms of model generalizability due to the dataset used. In our future

work, however, induration images from multi-racial and multi-ethnic sources, captured under substantially varied imaging conditions, will be used to improve the generalizability of the trained model.

6 DECLARATION OF COMPETING INTEREST

The authors declare that they have no known competing financial interests or personal relationships that could have appeared to influence the work reported in this paper.

7 ACKNOWLEDGEMENT

EA is supported through the 2023 Google Award for TensorFlow College Outreach

8 REFERENCES

[1] R. M. G. J. Houben, H. Esmail, F. Cobelens, C. M. L. Williams, and A. K. Coussens, "Tuberculosis prevalence: Beyond the tip of the iceberg," *The Lancet Respiratory Medicine,* vol. 10, no. 6, pp. 537–539, 2022. https://doi.org/10.1016/S2213-2600(22)00184-9

[2] H. Mohammed *et al.*, "Tuberculosis prevalence and predictors among health care-seeking people screened for cough of any duration in Ethiopia: A multicenter cross-sectional study," *Frontiers in Public Health,* vol. 9, 2022. https://doi.org/10.3389/fpubh.2021.805726

[3] J. Oyelade, I. Isewon, F. Aromolaran, and M. Achas, "Extreme pathway analysis of mycobacterium tuberculosis," in *International Conference on Computational Science and Computational Intelligence*, 2017, pp. 1270–1275. https://doi.org/10.1109/CSCI.2017.223

[4] L. L. L. Souza *et al.*, "Causes of multidrug-resistant tuberculosis from the perspectives of health providers: Challenges and strategies for adherence to treatment during the COVID-19 pandemic in Brazil," *BMC Health Serv. Res.*, vol. 21, 2021. https://doi.org/10.1186/s12913-021-07057-0

[5] S. Kiazyk and T. Ball, "Latent tuberculosis infection: An overview," *Canada Communicable Disease Report*, vol. 43, no. 3, pp. 62–66, 2017. https://doi.org/10.14745/ccdr.v43i34a01

[6] S. Rajaraman, L. R. Folio, J. Dimperio, P. O. Alderson, and S. K. Antani, "Improved semantic segmentation of tuberculosis—consistent findings in chest X-rays using augmented training of modality-specific U-Net models with weak localizations," *Diagnostics,* vol. 11, no. 4, p. 616, 2021. https://doi.org/10.3390/diagnostics11040616

[7] M. Singh, G. V. Pujar, S. A. Kumar, M. Bhagyalalitha, and H. S. Akshatha, "Evolution of machine learning in tuberculosis diagnosis: A review of deep learning-based medical applications," *Electronics*, vol. 11, no. 17, p. 2634, 2022. https://doi.org/10.3390/electronics11172634

[8] J. M. M. S. Pedro and D. P. Y. Barfeh, "Tuberculin skin test checker using digital image processing," in *3rd International Conference on Control and Robotics Engineering (ICCRE)*, Nagoya, Japan, 2018, pp. 233–237. https://doi.org/10.1109/ICCRE.2018.8376471

[9] Y. Yang and N. Xia, "Enhancing students' metacognition via AI-driven educational support *systems," International Journal of Emerging Technologies in Learning (iJET)*, vol. 18, no. 24, pp. 133–148, 2023. https://doi.org/10.3991/ijet.v18i24.45647

[10] Z. Li, "AI-assisted emotion recognition: Impacts on mental health education and learning motivation," *International Journal of Emerging Technologies in Learning (iJET)*, vol. 18, no. 24, pp. 34–48, 2023. https://doi.org/10.3991/ijet.v18i24.45645

[11] S. Issaro and P. Wannapiroon, "Intelligent student relationship management platform with machine learning for student empowerment," *International Journal of Emerging Technologies in Learning (iJET)*, vol. 18, no. 4, pp. 66–87, 2023. https://doi.org/10.3991/ijet.v18i04.32583

[12] Z. Kanetaki, C. Stergiou, G. Bekas, C. Troussas, and C. Sgouropoulou, "A hybrid machine learning model for grade prediction in online engineering education," *International Journal of Engineering Pedagogy (iJEP)*, vol. 12, no. 3, pp. 4–24, 2022. https://doi.org/10.3991/ijep.v12i3.23873

[13] S. Assami, N. Daoudi, and R. Ajhoun, "Implementation of a machine learning-based MOOC recommender system using learner motivation prediction," *International Journal of Engineering Pedagogy (iJEP)*, vol. 12, no. 5, pp. 65–85, 2022. https://doi.org/10.3991/ijep.v12i5.30523

[14] M. Malatesta and E. Ciani, "SkillGym AI digital role play to support leadership soft skills development through practice: A case study," *International Journal of Advanced Corporate Learning (iJAC)*, vol. 15, no. 2, pp. 41–56, 2022. https://doi.org/10.3991/ijac.v15i2.34871

[15] A. H. Aljammal, A. Qawasmeh, A. Mughaid, S. Taamneh, F. I. Wedyan, and M. Obiedat, "Performance evaluation of machine learning approaches in detecting IoT-Botnet attacks," *International Journal of Interactive Mobile Technologies*, vol. 17, no. 19, pp. 136–146, 2023. https://doi.org/10.3991/ijim.v17i19.41379

[16] R. Jáuregui-Velarde, L. Andrade-Arenas, D. H. Celis, R. C. Dávila-Morán, and M. Cabanillas-Carbonell, "Web application with machine learning for house price prediction," *International Journal of Interactive Mobile Technologies*, vol. 17, no. 23, pp. 85–104, 2023. https://doi.org/10.3991/ijim.v17i23.38073

[17] K. Baba, N.-E. El-Faddouli, and N. Cheimanoff, "Mobile-optimized AI-driven personalized learning: A case study at Mohammed VI Polytechnic university," *International Journal of Interactive Mobile Technologies*, vol. 18, no. 4, pp. 81–96, 2024. https://doi.org/10.3991/ijim.v18i04.46547

[18] C. Kowald and B. Bruns, "Chatbot Kim: A digital tutor on AI," *International Journal of Advanced Corporate Learning*, vol. 13, no. 3, pp. 26–34, 2020. https://doi.org/10.3991/ijac.v13i3.17017

[19] M. Koivisto, "Tutoring postgraduate students with an AI-based chatbot," *International Journal of Advanced Corporate Learning*, vol. 16, no. 1, pp. 41–54, 2023. https://doi.org/10.3991/ijac.v16i1.35437

[20] O. Aromolaran *et al.*, "Predicting host dependency factors of pathogens in Drosophila melanogaster using machine learning," *Computational and Structural Biotechnology Journal*, vol. 19, pp. 4581–4592, 2021. https://doi.org/10.1016/j.csbj.2021.08.010

[21] D. O. Enoma, J. Bishung, T. Abiodun, O. Ogunlana, and V. C. Osamor, "Machine learning approaches to genomewide association studies," *Journal of King Saud University – Science*, vol. 34, no. 4, p. 101647, 2022. https://doi.org/10.1016/j.jksus.2022.101847

[22] I. Lasri, N. El-Marzouki, A. Riadsolh, and M. Elbelkacemi, "Automated detection of dental caries from oral images using deep convolutional neural networks," *International Journal of Online and Biomedical Engineering (iJOE)*, vol. 19, no. 18, pp. 53–70, 2023. https://doi.org/10.3991/ijoe.v19i18.45133

[23] A. D. Orjuela-Cañón, A. L. Jutinico, C. Awad, E. Vergara, and A. Palencia, "Machine learning in the loop for tuberculosis diagnosis support," *Frontiers in Public Health*, vol. 10, pp. 1–10, 2022. https://doi.org/10.3389/fpubh.2022.876949

[24] A. M. Shabut *et al.*, "An intelligent mobile-enabled expert system for tuberculosis disease diagnosis in real time," *Expert Systems with Applications*, vol. 114, pp. 65–77, 2018. https://doi.org/10.1016/j.eswa.2018.07.014

[25] S. Naraghi, T. Mutsvangwa, R. Goliath, M. X. Rangaka, and T. S. Douglas, "Mobile phone-based evaluation of latent tuberculosis infection: Proof of concept for an integrated image capture and analysis system," *Computers in Biology and Medicine*, vol. 98, pp. 76–84, 2018. https://doi.org/10.1016/j.compbiomed.2018.05.009

[26] S. R. Rahayu *et al.*, "Development of the SIKRIBO mobile health application for active tuberculosis case detection in Semarang, Indonesia," *Healthcare Informatics Research*, vol. 28, no. 4, pp. 297–306, 2022. https://doi.org/10.4258/hir.2022.28.4.297

[27] R. Dendere, T. Mutsvangwa, R. Goliath, M. X. Rangaka, I. Abubakar, and T. S. Douglas, "Measurement of skin induration size using smartphone images and photogrammetric reconstruction: Pilot study," *JMIR Biomedical Engineering*, vol. 2, no. 1, p. e3, 2017. https://doi.org/10.2196/biomedeng.8333

[28] Y. Zhan, Y. Wang, W. Zhang, B. Ying, and C. Wang, "Diagnostic accuracy of the artificial intelligence methods in medical imaging for pulmonary tuberculosis: A systematic review and meta-analysis," *Journal of Clinical Medicine*, vol. 12, no. 1, p. 303, 2022. https://doi.org/10.3390/jcm12010303

[29] C. Prasitpuriprecha, S. S. Jantama, and T. Preeprem, "Drug-resistant tuberculosis treatment recommendation, and multi-class tuberculosis detection and classification using ensemble deep learning-based system," *Pharmaceuticals*, vol. 16, no. 1, p. 13, 2023. https://doi.org/10.3390/ph16010013

[30] R. Mohan, S. Kadry, V. Rajinikanth, A. Majumdar, and O. Thinnukool, "Automatic detection of tuberculosis using VGG19 with Seagull-Algorithm," *Life*, vol. 12, no. 11, p. 1848, 2022. https://doi.org/10.3390/life12111848

[31] M. Zachariou, O. Arandjelovi, W. Sabiiti, B. Mtafya, and D. Sloan, "Tuberculosis bacteria detection and counting in fluorescence microscopy images using a multi-stage deep learning pipeline," *Information*, vol. 13, no. 2, p. 96, 2022. https://doi.org/10.3390/info13020096

[32] S.-J. Heo, Y. Kim, L. S.-S. Yun, and J. Kim, "Deep learning algorithms with demographic information help to detect tuberculosis in chest," *International Journal of Environmental Research and Public Health*, vol. 16, no. 2, p. 250, 2019. https://doi.org/10.3390/ijerph16020250

[33] A. I. Lavrova and E. B. Postnikov, "An improved diagnostic of the mycobacterium tuberculosis drug resistance status by applying a decision tree to probabilities assigned by the CatBoost multiclassifier of matrix metalloproteinases biomarkers," *Diagnostics*, vol. 12, no. 11, pp. 2847, 2022. https://doi.org/10.3390/diagnostics12112847

[34] I. Haq, T. Mazhar, Q. Nasir, and Razzaq, "Machine vision approach for diagnosing tuberculosis (TB) based on computerized tomography (CT) scan images," vol. 14, no. 10, p. 1997, 2022. https://doi.org/10.3390/sym14101997

[35] M. H. L. F. Da Silva Barros *et al.*, "Benchmarking machine learning models to assist in the prognosis of tuberculosis," *Informatics*, vol. 8, no. 2, p. 27, 2021. https://doi.org/10.3390/informatics8020027

[36] B. Teahan, E. Ong, and Z. Yang, "Identification of mycobacterium tuberculosis antigens with vaccine potential using a machine learning-based reverse vaccinology approach," *Vaccine*, vol. 9, no. 10, p. 1098, 2021. https://doi.org/10.3390/vaccines9101098

[37] E. Kotei and R. Thirunavukarasu, "Ensemble technique coupled with deep transfer learning framework for automatic detection of tuberculosis from chest X-ray radiographs," *Healthcare*, vol. 10, no. 11, p. 2335, 2022. https://doi.org/10.3390/healthcare10112335

[38] O. Hrizi *et al.*, "Tuberculosis disease diagnosis based on an optimized machine learning model," *Journal of Healthcare Engineering*, vol. 2022, no.1, p. 8950243, 2022. https://doi.org/10.1155/2022/8950243

[39] X. A. Inbaraj, C. Villavicencio, J. J. Macrohon, J.-H. Jeng, and J.-G. Hsieh, "A novel machine learning approach for tuberculosis segmentation and prediction using chest-X-Ray (CXR) images," *Applied Sciences*, vol. 11, no. 19, p. 9057, 2021. https://doi.org/10.3390/app11199057

[40] R. B. Jeyavathana, G. Kalpana, and K. Kanimozhi, "An improved random forest approach for predicting tuberculosis," *European Journal of Molecular and Clinical Medicine*, vol. 7, no. 5, pp. 1739–1744, 2022.

[41] A. G. Green *et al.*, "A convolutional neural network highlights mutations relevant to antimicrobial resistance in Mycobacterium tuberculosis," *Nature Communications*, vol. 13, p. 3817, 2022. https://doi.org/10.1038/s41467-022-31236-0

[42] L. A. Andika, H. Pratiwi, and S. S. Handajani, "Convolutional neural network modeling for classification of pulmonary tuberculosis disease," *Journal of Physics: Conference Series*, vol. 1490, p. 012020, 2020. https://doi.org/10.1088/1742-6596/1490/1/012020

[43] S. F. Rabby, A. Hasan, Md. J. A. Soeb, G. P. Shirsho, and B. Talukdar, "Performance analysis of different Convolutional Neural Network (CNN) models with optimizers in detecting Tuberculosis (TB) from various chest X-ray images," *European Journal of Engineering and Technology Research*, vol. 7, no. 4, pp. 21–30, 2022. https://doi.org/10.24018/ejeng.2022.7.4.2861

[44] M. Oloko-Oba and S. Viriri, "Diagnosing tuberculosis using deep convolutional neural network," in *9th International Conference on Image and Signal Processing*, Marrakesh, Morocco, vol. 12119, 2019, pp. 151–161. https://doi.org/10.1007/978-3-030-51935-3_16

[45] J. D. Shaid, "Streamlit 101: An in-depth introduction," [Online].

[46] P. Iakubovskii, "Segmentation models," GitHub, 2019. [Online]. Available: https://github.com/qubvel/segmentation_models [Accessed 2022].

[47] M. Tan and Q. Le, "EfficientNet: Rethinking model scaling for convolutional neural networks," in *36th International Conference on Machine Learning*, Long Beach, 2019.

[48] F. Chollet, "Keras," GitHub, 2015. [Online]. Available: https://github.com/fchollet/keras [Accessed 2022].

[49] G. Bradski, "The OpenCV library," *Dr. Dobb's Journal of Software Tools*, vol. 120, pp. 122–125, 2000.

[50] C. Shorten and T. M. Khoshgoftaar, "A survey on image data augmentation for deep learning," *Journal of Big Data*, vol. 6, p. 60, 2019. https://doi.org/10.1186/s40537-019-0197-0

[51] O. Ronneberger, P. Fischer, and T. Brox, "U-Net: Convolutional networks for bio-medical image segmentation," in *Medical Image Computing and Computer-Assisted Intervention (MICCAI)*, 2015, pp. 234–241. https://doi.org/10.1007/978-3-319-24574-4_28

[52] Wikipedia, "ATM card," 2021. [Online]. Available: https://en.wikipedia.org/w/index.php?title=ATM_card&oldid=1021928801 [Accessed 2022].

[53] C. E. Nwankpa, W. L. Ijomah, A. Gachagan, and S. Marshall, "Activation functions: Comparison of trends in practice and research for deep learning," in *2nd International Conference on Computational Sciences and Technology*, Jamshoro, Pakistan, 2021.

[54] R. Adrian, "Measuring size of objects in an image with OpenCV," *PyImageSearch*, 2016. [Online]. [Accessed 2023].

9 AUTHORS

Olubunmi Adewale Akinola received the Bachelor, Masters, and Ph.D. degrees in Electrical Engineering in 1991, 2001, and 2016, respectively. He is currently at the Federal University of Agriculture, Abeokuta, Nigeria. He was the recipient of a plethora of research-based awards issued by the OMICS Group (USA) and NUC (Nigeria), just to mention a few. He is a member of the Nigerian Society of Engineers

and a registered engineer with the Council for the Regulation of Engineering in Nigeria (COREN). His research interests include AI in health care, IoT, D2D communications, MANETS, automation, and electronic system design and applications (E-mail: akinolaoa@funaab.edu.ng).

Joseph Folorunsho Orimolade obtained his B.Eng. and M.Sc. degrees in Electrical Engineering from Ahmadu Bello University, Zaria, Nigeria. He worked in the capacity of a senior engineer, lecturer, and researcher at different Universities, including Ahmadu Bello University, Zaria Nigeria, the Federal University of Agriculture, Abeokuta Nigeria, and Saint Francis University (CIHE), Hong Kong, among others. He obtained a Doctor of Philosophy (PhD) in Electrical Engineering from the University of Cape Town, South Africa, where he majors in wireless communications and networking. His research contributions have been presented at international conferences and journal proceedings. Current research interests are in the areas of radio resources management in 5G/6G wireless networks and applications of AI in health care (E-mail: jorimolade@cihe.edu.hk).

Akindele Segun Afolabi received his Bachelor and Master's Degrees in Electrical Engineering from the University of Ilorin, Nigeria, and his Ph.D. Degree in Computer Science and Systems Engineering from Kobe University, Japan. He was the recipient of the prestigious Japanese Government MEXT Scholarship Award from 2009 to 2012. He is currently at the University of Ilorin, and he is fully registered with the Council for the Regulation of Engineering in Nigeria (COREN). His research interests include wireless sensor networks, the Internet of Things, VANET, D2D communications, and artificial intelligence (E-mail: afolabisegun@unilorin.edu.ng).

Habeeb Kehinde Shopeju is a machine learning research engineer at Thomson Reuters Labs, UK. With a degree in Electrical Electronics Engineering from the Federal University of Agriculture, Abeokuta, he currently focuses on doing research and building products for the Machine Learning and Information Retrieval domain (E-mail: habeeb.shopeju@thomsonreuters.com).

Emmanuel Adetiba (Member, IEEE) obtained a Ph.D. degree in Information and Communication Engineering from Covenant University, Ota, Nigeria. He is a registered engineer (R.Engr.) with the Council for the Regulation of Engineering in Nigeria (COREN) and a member of the Institute of Information Technology Professionals (IITP), South Africa, as well as the Institute of Electrical and Electronics Engineering (IEEE), USA. He is a recipient of several past and ongoing scholarly grants and funds from reputable bodies such as the World Bank, France Development Agency (AFD), Google, the US National Science Foundation, Durban University of Technology in South Africa, the Nigeria Communications Commission, the Rockefeller Foundation, the International Medical Informatics Association (IMIA), and a host of others. He has authored or co-authored more than 100 scholarly publications in journals and conference proceedings, some of which are indexed in Scopus/ISI/CPCI. His research interests and experiences include machine intelligence, software-defined radio, cognitive radio, biomedical signal processing, and cloud and high performance computing (C&HPC). He was the Director at the Center for Systems and Information Services (aka ICT Center), Covenant University, from 2017 to 2019. He is an incumbent Deputy Director at the Covenant Applied Informatics and Communication Africa Centre of Excellence (CApIC-ACE) and Principal Investigator for the FEDGEN cloud computing research project at the center (World Bank and AFD-funded). He is the founder and principal investigator of the Advanced Signal Processing and Machine Intelligence Research (ASPMIR) Group (www.aspmir.net). He is a full professor and former head of the Department of Electrical and Information Engineering at Covenant University (2021–2023). He is also an Honorary Research Associate (HRA)

at the Institute of System Sciences and a Visiting Professor at the KZN eSkills CoLab, Durban University of Technology, Durban, South Africa (E-mail: emmanuel.adetiba@covenantuniversity.edu.ng).

Adeyinka Ajao Adewale is an Associate Professor in the Department of Electrical and Information Engineering, College of Engineering, Covenant University. He is a Ph.D. degree holder in information and communication engineering with a background in electrical engineering. He is a COREN registered engineer and a corporate member of the Nigerian Society of Engineers (NSE) and has a number of professional qualifications to his credit. His research area of focus includes quality of service (QoS) in mobile or wireless communication; IP mobility; network convergence (IP next generation); computer and communication network design; network planning and optimization; software design and programming; and artificial intelligence (E-mail: ade.adewale@covenantuniversity.edu.ng).

Copyright of International Journal of Online & Biomedical Engineering is the property of International Journal of Online Engineering and its content may not be copied or emailed to multiple sites or posted to a listserv without the copyright holder's express written permission. However, users may print, download, or email articles for individual use.